# Constraining URCA cooling of neutron stars from the neutron radius of $^{208}$Pb

C. J. Horowitz*
*Department of Physics and Nuclear Theory Center, Indiana University, Bloomington, Indiana 47405*

J. Piekarewicz†
*Department of Physics, Florida State University, Tallahassee, Florida 32306*
(Received 24 July 2002; published 27 November 2002)

Recent observations by the Chandra observatory suggest that some neutron stars may cool rapidly, perhaps by the direct URCA process which requires a high proton fraction. The proton fraction is determined by the nuclear symmetry energy whose density dependence may be constrained by measuring the neutron radius of a heavy nucleus, such as $^{208}$Pb. Such a measurement is necessary for a reliable extrapolation of the proton fraction to the higher densities present in a neutron star. A large neutron radius in $^{208}$Pb implies a stiff symmetry energy that grows rapidly with density, thereby favoring a high proton fraction and allowing direct URCA cooling. Predictions for the neutron radius in $^{208}$Pb are correlated to the proton fraction in dense matter by using a variety of relativistic effective field-theory models. Models that predict a neutron ($R_n$) minus proton ($R_p$) root-mean-square radius in $^{208}$Pb to be $R_n - R_p \lesssim 0.20$ fm have proton fractions too small to allow the direct URCA cooling of $1.4M_\odot$ neutron stars. Conversely, if $R_n - R_p \gtrsim 0.25$ fm, the direct URCA process is allowed (by all models) to cool down a $1.4M_\odot$ neutron star. The Parity Radius Experiment at Jefferson Laboratory aims to measure the neutron radius in $^{208}$Pb accurately and model independently via parity-violating electron scattering. Such a measurement would greatly enhance our ability to either confirm or dismiss the direct URCA cooling of neutron stars.

DOI: 10.1103/PhysRevC.66.055803 PACS number(s): 26.60.+c, 21.10.Gv

## I. INTRODUCTION

Neutron stars are created with very high temperatures in supernova explosions. Indeed, neutrinos observed from SN1987A indicate a neutrinosphere temperature that could be as high as 5 MeV [1]. Neutrons stars then cool, primarily by neutrino emission [2]. In the standard scenario, the modified URCA reaction

$$n + n \rightarrow n + p + e^- + \overline{\nu}_e \tag{1}$$

emits neutrinos from the volume of the star. This process, however, is relatively slow as a second nucleon is necessary to conserve momentum.

Recent x-ray observations of the neutron star in 3C58 [3], Vela [4], and Geminga [5] indicate low surface temperatures. Moreover, the low quiescent luminosity in the transiently accreting binaries KS 1731-260 [6] and Cen X-4 [7] suggest rapid cooling. As x-ray observatories progress and our knowledge of neutron-star atmospheres and ages improves, additional ''cold'' neutron stars may be discovered. Such low surface temperatures appear to require enhanced cooling from reactions that proceed faster than the modified URCA process of Eq. (1).

Measuring the surface temperature of neutron stars is difficult as their surface temperatures can be anisotropic. Moreover, the extracted surface temperature can depend significantly on the model atmosphere employed. Finally, many neutron stars, such as RX J0822-4300 [8], appear warm and fully consistent with modified URCA cooling.

Enhanced cooling may occur via the weak decay of additional hadrons such as pion or kaon condensates [9], hyperons [10], or quark matter [11]. Yet perhaps the most conservative enhanced-cooling mechanism is the direct URCA process [12,13] of neutron beta decay followed by electron capture:

$$n \rightarrow p + e^- + \overline{\nu}_e , \tag{2a}$$

$$e^- + p \rightarrow n + \nu_e . \tag{2b}$$

This mechanism is not ''exotic'' as it only requires protons, neutrons, and electrons—constituents known to be present in dense matter. However, to conserve momentum in Eq. (2a) the sum of the Fermi momenta of the protons plus that of the electrons must be greater than (or equal to) the neutron Fermi momentum. This requires a relatively large proton fraction.

Yakovlev and collaborators [14] are able to reproduce measured neutron-star temperatures using a relativistic mean-field equation of state that allows direct URCA for neutron stars with masses above $1.358M_\odot$ ($M_\odot$ = solar mass). In contrast, Tsuruta and collaborators [15] rely on pion condensation to reproduce the measured temperatures. They argue that microscopic calculations of neutron-rich matter [16] using nonrelativistic nucleon-nucleon interactions yield too small a proton fraction for the URCA process to operate. Unfortunately, these microscopic calculations depend on a poorly known three-nucleon force and on relativistic effects that could end up increasing the proton fraction at high densities.

*Electronic address: horowitz@iucf.indiana.edu
†Electronic address: jorgep@csit.fsu.edu

 

Superconductivity and superfluidity can greatly influence neutron-star cooling [17,18]. For temperatures much lower than the pairing gap, pairing correlations suppress exponentially the rate of many cooling reactions. Yet for temperatures of the order of the pairing gap, the thermal breaking and subsequent reformation of nucleon ''Cooper'' pairs promotes an additional neutrino-emission mechanism that rapidly cools the star [19]. However, it has been argued in Ref. [14] that this mechanism alone is unlikely to explain the low temperature of some neutron stars. This is because for a large enough neutron-pairing gap, pair breaking would rapidly cool all neutron stars at a rate almost independent of the mass of the star. This would disagree with observations of some warm neutron stars. Tsuruta and Tamagaki have claimed that microscopic calculations with a high proton concentration show a small proton pairing gap [20]. If so, a direct URCA process (one not controlled by pairing correlations) will cool a star so quickly that thermal radiation would become invisible [15]. However, we caution that drawing definitive conclusions from microscopic calculations of pairing gaps may be premature, as significant uncertainties remain in the interactions, equation of state, composition, and phases of high-density matter.

Although the precise mechanism remains unknown, some kind of enhanced cooling appears to be required to explain the recent observations of cold neutron stars. While the need for exotic phases of matter is appealing, more conventional cooling scenarios, such as the direct URCA process, cannot be dismissed on purely theoretical grounds. Moreover, neutron-star observations alone may not be able to resolve the detailed mechanism of enhanced cooling. Thus, we consider complementary laboratory experiments that could help us confirm (or possibly dismiss) the direct URCA process. This can be achieved by constraining the symmetry energy of dense matter. The symmetry energy describes how the energy of (asymmetric) nuclear matter increases as one departs from equal numbers of neutrons and protons. The proton fraction $Y_p = Z/A$ of nuclear matter in beta equilibrium is sensitive to the symmetry energy [12]. A large symmetry energy imposes a stiff penalty on the system for upsetting the $N = Z$ balance, thereby forcing it to retain a large proton fraction.

Energetic heavy-ion collisions probe the symmetry energy at high nuclear densities [21]. Possible observables include the ratio of $\pi^-$-to-$\pi^+$ production and the neutron-proton differential collective flow. However, these reactions may suffer from important uncertainties associated with the complex strong interactions of the heavy-ion collisions. Thus, we rely on a purely electroweak reaction that can be unambiguously interpreted. Parity-violating elastic electron scattering from a heavy nucleus is sensitive to the neutron density. This is because the weak charge of a neutron is much larger than the weak charge of a proton. The Parity Radius Experiment at the Jefferson Laboratory aims to measure the neutron radius in $^{208}$Pb to a 1% accuracy ($\pm 0.05$ fm) [22]. This measurement can be both accurate and model independent [23]. While the experiment has been approved, it awaits the completion of other parity-violating experiments, using hydrogen and helium targets, which make use of the same beamline. In Ref. [24] Brown showed that the neutron radius of $^{208}$Pb determines the pressure of neutron-rich matter at normal densities which, in turn, is related to the density dependence of the symmetry energy [25]. The binding energy of neutron-rich nuclei is also sensitive to the symmetry energy. Thus, mass measurements of exotic nuclei at newly commissioned radioactive beam facilities could provide complimentary information. However, one should note that in addition to being sensitive to a variety of nuclear-structure properties, the binding energy of neutron-rich nuclei is fairly insensitive to the density dependence of the symmetry energy [26]. In an earlier work we showed how the neutron radius of $^{208}$Pb determines properties of the neutron-star surface, such as the transition density from a solid crust to a liquid interior [27]. Furthermore, we argued that by comparing the neutron radius of $^{208}$Pb (a low-density observable) to the radius of a neutron star (a high- and low-density observable) evidence may be provided in support of a phase transition in dense matter [28].

In the present work we show how the neutron radius of a heavy nucleus (such as $^{208}$Pb) controls the density dependence of the symmetry energy. Unfortunately, the density dependence of the symmetry energy ($da_{\rm sym}/d\rho$) is poorly known. Thus a measurement of the neutron radius of $^{208}$Pb seems vital, as it will constrain the density dependence of the symmetry energy at low density. This, in turn, will allow a more reliable extrapolation of the symmetry energy and thus a more reliable determination of the proton fraction at the higher densities required in the study of neutron-star structure. While in principle collective modes of nuclei, such as the giant-dipole or isovector-monopole resonances, are sensitive to $da_{\rm sym}/d\rho$, in practice this sensitivity is small. Moreover, the parameter sets used in the calculations (see various tables) have been adjusted so that well-known ground-state properties remain fixed while changing the neutron radius. This shows that existing ground-state information, such as charge densities or binding energies, does not determine the neutron radius uniquely. Thus the need for a new measurement—such as the neutron radius in $^{208}$Pb—that will provide important information on $da_{\rm sym}/d\rho$.

The paper has been organized as follows. In Sec. II, relativistic effective-field theories for both dense matter and finite nuclei are discussed. A large number of parameter sets are considered so that the density dependence of the symmetry energy may be changed while reproducing existing ground-state data. In Sec. III, results for the equilibrium proton fraction as a function of baryon density are presented using interactions that predict different neutron radii in $^{208}$Pb. Our summary and conclusions are offered in Sec. IV. In particular, we conclude that for models with a large neutron skin in $^{208}$Pb ($R_n - R_p \gtrsim 0.25$ fm) the symmetry energy rises rapidly with density and the direct URCA cooling of a $1.4M_\odot$ neutron star is likely. Conversely, if the neutron radius is small ($R_n - R_p \lesssim 0.20$ fm), it is unlikely that the direct URCA process occurs. In this case, the enhanced cooling of neutron stars may indeed require the presence of exotic states of matter, such as meson condensates, hyperonic, and/or quark matter.

## II. FORMALISM

Our starting point will be the relativistic effective-field theory of Ref. [29] supplemented with additional couplings between the isoscalar and isovector mesons. This allows us to correlate nuclear observables sensitive to the density dependence of the symmetry energy, such as the neutron radius of $^{208}$Pb, with neutron-star properties, such as the threshold mass for URCA cooling. As the density dependence of the symmetry energy is poorly known, uncertainties in these correlations will be explored by considering a wide range of model parameters. The interacting Lagrangian density is thus given by [27,29]

$$\mathcal{L}_{\rm int}=\bar{\psi}\left[g_{\rm s}\phi-\left(g_{\rm v}V_{\mu}+\frac{g_{\rho}}{2}\boldsymbol{\tau}\cdot\mathbf{b}_{\mu}+\frac{e}{2}(1+\tau_3)A_{\mu}\right)\gamma^{\mu}\right]\psi$$
$$-\frac{\kappa}{3!}(g_{\rm s}\phi)^3-\frac{\lambda}{4!}(g_{\rm s}\phi)^4+\frac{\zeta}{4!}g_{\rm v}^4(V_{\mu}V^{\mu})^2$$
$$+g_{\rho}^2\,\mathbf{b}_{\mu}\cdot\mathbf{b}^{\mu}[\Lambda_{\rm s}g_{\rm s}^2\phi^2+\Lambda_{\rm v}g_{\rm v}^2V_{\mu}V^{\mu}]. \tag{3}$$

The model contains an isodoublet nucleon field ($\psi$) interacting via the exchange of two isoscalar mesons, the scalar sigma ($\phi$) and the vector omega ($V^{\mu}$), one isovector meson, the rho ($\mathbf{b}^{\mu}$), and the photon ($A^{\mu}$). In addition to meson-nucleon interactions the Lagrangian density includes scalar and vector self-interactions. The scalar-meson self-interactions ($\kappa$ and $\lambda$) soften the equation of state (EOS) of symmetric nuclear matter at (and near) saturation density while the $\omega$-meson self-interactions ($\zeta$) soften the high-density component of the EOS. Finally, the nonlinear couplings ($\Lambda_{\rm s}$ and $\Lambda_{\rm v}$) are included to modify the density dependence of the symmetry energy [27,28].

The energy of neutron-rich matter may be written in terms of the energy of symmetric nuclear matter ($\rho_p=\rho_n$) and the symmetry energy $a_{\rm sym}(\rho)$. That is,

$$\frac{E}{A}(\rho,t)=\frac{E}{A}(\rho,t=0)+t^2a_{\rm sym}(\rho)+\mathcal{O}(t^4), \tag{4}$$

where the neutron excess has been defined as

$$t\equiv\frac{\rho_n-\rho_p}{\rho_n+\rho_p}. \tag{5}$$

Here $\rho_n$ is the neutron and $\rho_p$ the proton density, and

$$\rho=\rho_p+\rho_n\equiv\frac{2k_{\rm F}^3}{3\pi^2}. \tag{6}$$

The symmetry energy describes how the energy of the system increases as one moves away from $\rho_p=\rho_n$. It is discussed in Ref. [28] where it is shown that it is given by

$$a_{\rm sym}(\rho)=\frac{k_F^2}{6E_F^*}+\frac{g_{\rho}^2}{12\pi^2}\frac{k_F^3}{m_{\rho}^{*2}}, \tag{7}$$

where $k_{\rm F}$ is the Fermi momentum, $E_F^*=\sqrt{k_{\rm F}^2+M^{*2}}$, and $M^*=M-g_s\phi_0$ is the effective nucleon mass. Further, the effective rho-meson mass has been defined as follows:

$$m_{\rho}^{*2}=m_{\rho}^2+2g_{\rho}^2(\Lambda_{\rm s}g_{\rm s}^2\phi_0^2+\Lambda_{\rm v}g_{\rm v}^2V_0^2). \tag{8}$$

The symmetry energy is given as a sum of two contributions. The first term in Eq. (7) represents the increase in the kinetic energy of the system due to the displacement of the Fermi levels of the two species (neutrons and protons). This contribution has been fixed by the properties of symmetric nuclear matter as it only depends on the nucleon effective mass $M^*$. By itself, it leads to an unrealistically low value for the symmetry energy; for example, at saturation density this contribution yields $\sim$15 MeV, rather than the most realistic value of $\sim$37 MeV. The second contribution is due to the coupling of the rho meson to an isovector-vector current that no longer vanishes in the $N\neq Z$ system. It is by adjusting the strength of the $NN\rho$ coupling constant that one can now fit the empirical value of the symmetry energy at saturation density. However, the symmetry energy at saturation is not well constrained experimentally. Yet an average of the symmetry energy at saturation density and the surface symmetry energy is constrained by the binding energy of nuclei. Thus, the following prescription is adopted: the value of the $NN\rho$ coupling constant is adjusted so that all parameter sets have a symmetry energy of $a_{\rm sym}=25.67$ MeV at $k_F=1.15$ fm$^{-1}$($\rho=0.10$ fm$^{-3}$) [27]. That is,

$$g_{\rho}^2=\frac{m_{\rho}^2\;\Delta a_{\rm sym}}{\dfrac{k_F^3}{12\pi^2}-2(\Lambda_{\rm s}g_{\rm s}^2\phi_0^2+\Lambda_{\rm v}g_{\rm v}^2V_0^2)\Delta a_{\rm sym}}, \tag{9}$$

where $\Delta a_{\rm sym}\equiv(a_{\rm sym}-k_F^2/6E_F^*)$. This prescription ensures accurate binding energies for heavy nuclei, such as $^{208}$Pb. Following this prescription the symmetry energy at saturation density is predicted (for $\Lambda_{\rm s}=\Lambda_{\rm v}=0$) to be 37.3, 36.6, and 36.3 MeV for the three families of parameter sets considered in this work: namely, NL3 [30], S271 [27], and Z271 [27], respectively (see various tables). Moreover, all these parameter sets reproduce the following properties of symmetric nuclear matter: (i) nuclear saturation at a Fermi momentum of $k_{\rm F}=1.30$ fm$^{-1}$, with (ii) a binding energy per nucleon of 16.24 MeV, and (iii) a nuclear incompressibility of $K=271$ MeV. These values follow from the successful parametrization of Ref. [30] and, thus, have been adopted for the other sets (S271 and Z271) as well. Yet the various parameter sets differ in (i) their values for the effective nucleon mass at saturation density, (ii) the value of the $\omega$-meson quartic coupling ($\zeta\neq0$ for set Z271 but vanishes for the NL3 and S271 sets), and (iii) the nonlinear couplings $\Lambda_{\rm s}$ and $\Lambda_{\rm v}$ (see various tables). Note that changing $\Lambda_{\rm s}$ or $\Lambda_{\rm v}$ modifies the density dependence of the symmetry energy through a change in the effective rho-meson mass [see Eq. (8)]. In general, increasing either $\Lambda_{\rm s}$ or $\Lambda_{\rm v}$ causes the symmetry energy to soften—that is, to grow slower with increasing density. This, in turn, allows for a larger neutron-proton mismatch or, equivalently, for a lower equilibrium proton

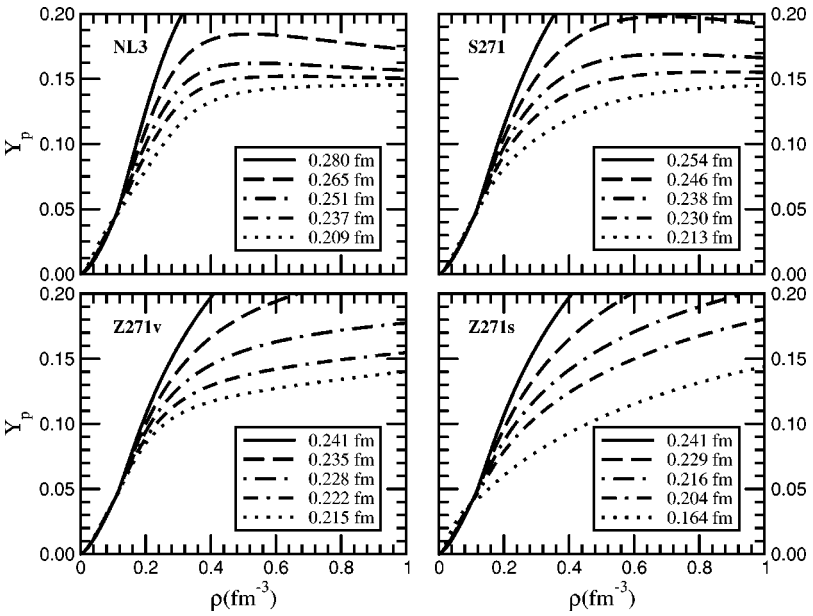


FIG. 1. Proton fraction $Y_p$ versus baryon density $\rho$ for neutron-rich matter in beta equilibrium for all parameter sets discussed in the text. For every given set, the curves represent different values of the isoscalar-isovector coupling ($\Lambda_v$ or $\Lambda_s$) that yield the values of $R_n - R_p$ indicated in the inset. See also the various tables in the text.

fraction at high density. The neutron radius of $^{208}$Pb also depends on the density dependence of the symmetry energy. A stiff density dependence (i.e., pressure) for neutron matter pushes neutrons out against surface tension, leading to a large neutron radius. The pressure of neutron-rich matter depends on the derivative of the energy of symmetric matter with respect to the density $[dE(\rho,t=0)/d\rho]$ and on the derivative of the symmetry energy $(da_{\rm sym}/d\rho)$. While the former is well known, at least in the vicinity of the saturation density, the latter is not. Hence, by changing the values of $\Lambda_s$ or $\Lambda_v$ one can adjust the density dependence of the symmetry energy $da_{\rm sym}/d\rho$, while keeping a variety of well-known ground-state properties (such as the proton radius and the binding energy of $^{208}$Pb) unchanged. Note that parameter sets with a large "pressure," $da_{\rm sym}/d\rho$, yield a large neutron radius in $^{208}$Pb.

## III. RESULTS

In this section results are presented for various observables that have been computed using an equation of state for matter composed of neutrons, protons, electrons, and muons in beta equilibrium:

$$n \leftrightarrow p + e^- + \overline{\nu}_e , \tag{10a}$$

TABLE I. Model parameters used in the calculations. The parameter $\kappa$ and the scalar mass $m_s$ are given in MeV. The nucleon, rho, and omega masses are kept fixed at $M=939$, $m_\rho=763$, and $m_\omega=783$ MeV, respectively—except in the case of the NL3 model where it is fixed at $m_\omega=782.5$ MeV.

| Model | $m_s$ | $g_s^2$ | $g_v^2$ | $\kappa$ | $\lambda$ | $\zeta$ |
|---|---|---|---|---|---|---|
| NL3 | 508.194 | 104.3871 | 165.5854 | 3.8599 | −0.01591 | 0.00 |
| S271 | 505.000 | 81.1071 | 116.7655 | 6.6834 | −0.01580 | 0.00 |
| Z271 | 465.000 | 49.4401 | 70.6689 | 6.1696 | +0.15634 | 0.06 |

$$e^- \leftrightarrow \mu^- + \nu_e + \overline{\nu}_\mu . \tag{10b}$$

These reactions demand that the chemical potential $(\mu)$ of the various constituents be related by the following equation:

$$\mu_n - \mu_p = \mu_e = \mu_\mu , \tag{11}$$

where $\mu_n$, $\mu_p$, $\mu_e$, and $\mu_\mu$ represent the chemical potentials of neutrons, protons, electrons, and muons, respectively. Neglecting the rest mass of the electron, Eq. (10b) is equivalent (for $k_F^e \geqslant m_\mu$) to the following equation expressed in terms of the Fermi momenta of the electron and muon:

$$k_F^e = \sqrt{(k_F^\mu)^2 + m_\mu^2}. \tag{12}$$

Finally, charge neutrality imposes the following constraint on the system: $\rho_p = \rho_e + \rho_\mu$ or, equivalently,

$$(k_F^p)^3 = (k_F^e)^3 + (k_F^\mu)^3. \tag{13}$$

TABLE II. Results for the NL3 parameter set with $\Lambda_s=0$. The neutron skin $(R_n - R_p)$ of $^{208}$Pb is given along with the threshold density for the direct URCA process $\rho_{\rm URCA}$, the corresponding proton fraction $Y_{p\ \rm URCA}$, and the minimum mass neutron star where the direct URCA process is the allowed $M_{\rm URCA}$. Note that $R_n - R_p$ is given in fm, $\rho_{\rm URCA}$ in fm$^{-3}$, and $M_{\rm URCA}$ in solar masses.

| $\Lambda_v$ | $g_\rho^2$ | $R_n - R_p$ | $\rho_{\rm URCA}$ | $Y_{p\ \rm URCA}$ | $M_{\rm URCA}$ |
|---|---|---|---|---|---|
| 0.0000 | 79.6 | 0.280 | 0.205 | 0.130 | 0.838 |
| 0.0050 | 84.9 | 0.266 | 0.233 | 0.131 | 0.944 |
| 0.0100 | 90.9 | 0.251 | 0.271 | 0.132 | 1.224 |
| 0.0125 | 94.2 | 0.244 | 0.293 | 0.133 | 1.435 |
| 0.0150 | 97.9 | 0.237 | 0.319 | 0.134 | 1.671 |
| 0.0200 | 106.0 | 0.223 | 0.376 | 0.135 | 2.123 |
| 0.0250 | 115.6 | 0.209 | 0.442 | 0.136 | 2.449 |

TABLE III. Results for the S271 parameter set with $\Lambda_s=0$. The neutron skin $(R_n-R_p)$ of $^{208}$Pb is given along with the threshold density for the direct URCA process $\rho_{\rm URCA}$, the corresponding proton fraction $Y_{p\ \rm URCA}$, and the minimum mass neutron star where the direct URCA process is the allowed $M_{\rm URCA}$. Note that $R_n-R_p$ is given in fm, $\rho_{\rm URCA}$ in fm$^{-3}$, and $M_{\rm URCA}$ in solar masses.

| $\Lambda_v$ | $g_\rho^2$ | $R_n-R_p$ | $\rho_{\rm URCA}$ | $Y_{p\ \rm URCA}$ | $M_{\rm URCA}$ |
|---|---|---|---|---|---|
| 0.000 | 85.4357 | 0.254 | 0.224 | 0.130 | 0.830 |
| 0.005 | 88.3668 | 0.246 | 0.252 | 0.132 | 0.894 |
| 0.010 | 91.5061 | 0.238 | 0.296 | 0.133 | 1.059 |
| 0.015 | 94.8767 | 0.230 | 0.374 | 0.135 | 1.429 |
| 0.020 | 98.5051 | 0.221 | 0.501 | 0.137 | 1.938 |
| 0.025 | 102.4221 | 0.214 | 0.663 | 0.139 | 2.248 |
| 0.030 | 106.6635 | 0.205 | 0.843 | 0.140 | 2.343 |

TABLE V. Results for the Z271 parameter set with $\Lambda_v=0$. The neutron skin $(R_n-R_p)$ of $^{208}$Pb is given along with the threshold density for the direct URCA process $\rho_{\rm URCA}$, the corresponding proton fraction $Y_{p\ \rm URCA}$, and the minimum mass neutron star where the direct URCA process is the allowed $M_{\rm URCA}$. Note that $R_n-R_p$ is given in fm, $\rho_{\rm URCA}$ in fm$^{-3}$, and $M_{\rm URCA}$ in solar masses.

| $\Lambda_s$ | $g_\rho^2$ | $R_n-R_p$ | $\rho_{\rm URCA}$ | $Y_{p\ \rm URCA}$ | $M_{\rm URCA}$ |
|---|---|---|---|---|---|
| 0.000 | 90.2110 | 0.241 | 0.242 | 0.131 | 0.816 |
| 0.010 | 96.3974 | 0.229 | 0.287 | 0.133 | 0.901 |
| 0.020 | 103.4949 | 0.216 | 0.366 | 0.135 | 1.078 |
| 0.030 | 111.7205 | 0.204 | 0.488 | 0.137 | 1.300 |
| 0.040 | 121.3666 | 0.191 | 0.636 | 0.139 | 1.467 |
| 0.050 | 132.8358 | 0.178 | 0.789 | 0.140 | 1.560 |
| 0.060 | 146.6988 | 0.164 | 0.936 | 0.141 | 1.605 |

For a given proton Fermi momentum, the corresponding Fermi momenta for the electrons and the muons are readily obtained by solving Eqs. (12) and (13). With these in hand, Eq. (11) determines the equilibrium neutron $(Y_n=N/A)$ and proton $(Y_p=Z/A)$ fractions in the system.

In Fig. 1 the proton fraction $Y_p$ for matter in beta equilibrium is shown as a function of the baryon density for all models discussed in the text (see Table I). The various curves displayed in each panel are for values of $\Lambda_s$ or $\Lambda_v$ that give the indicated values for the neutron skin of $^{208}$Pb. Note that the neutron skin of a nucleus is defined as the difference between the neutron $(R_n)$ and proton $(R_p)$ root-mean-square radii. All of the curves yield the same proton fraction at low density ($k_F=1.15$ fm$^{-1}$ or $\rho\approx 0.1$ fm$^{-3}$) because the symmetry energy has been adjusted to $a_{\rm sym}=25.67$ MeV in order to reproduce the binding energy $^{208}$Pb. The proton fraction increases more rapidly with density for those parameter sets that yield larger neutron radii in $^{208}$Pb (namely, those with a stiffer symmetry energy). Thus, the neutron radius of $^{208}$Pb constrains the slope $dY_p/d\rho$ at normal densities. This enables one to make a more reliable extrapolation of $Y_p$ to the higher densities where it displays some model dependence.

The direct URCA process is viable only when the proton fraction is large enough to conserve momentum in the neutron beta decay reaction of Eq. (2a). Hence, for this reaction to proceed, the Fermi momenta of neutrons, protons, and electrons must satisfy the following relation:

$$k_F^n \leqslant k_F^p + k_F^e. \tag{14}$$

The URCA threshold density $\rho_{\rm URCA}$ is defined as the density at which the equality $(k_F^n=k_F^p+k_F^e)$ is satisfied. Note that in the simplified case of matter without muons—that is, $k_F^e<m_\mu$ and $k_F^p=k_F^e$—the proton fraction at the onset of the direct URCA process is $Y_p=1/9\sim 0.111$. In the opposite limit, $k_F^e \gg m_\mu$, the threshold proton fraction is $Y_p\sim 0.148$. Thus, the threshold proton fraction must be contained within these two values for all baryon densities (see Tables II–V). In Fig. 2 the URCA threshold density is displayed as a function of the neutron skin $R_n-R_p$ of $^{208}$Pb. There is a clear tendency for $\rho_{\rm URCA}$ to decrease with increasing neutron skin. Recall that a large neutron skin implies a stiff symmetry energy and a large proton fraction. Thus the onset for the direct URCA process for models with large neutron skins

TABLE IV. Results for the Z271 parameter set with $\Lambda_s=0$. The neutron skin $(R_n-R_p)$ of $^{208}$Pb is given along with the threshold density for the direct URCA process $\rho_{\rm URCA}$, the corresponding proton fraction $Y_{p\ \rm URCA}$, and the minimum mass neutron star where the direct URCA process is the allowed $M_{\rm URCA}$. Note that $R_n-R_p$ is given in fm, $\rho_{\rm URCA}$ in fm$^{-3}$, and $M_{\rm URCA}$ in solar masses.

| $\Lambda_v$ | $g_\rho^2$ | $R_n-R_p$ | $\rho_{\rm URCA}$ | $Y_{p\ \rm URCA}$ | $M_{\rm URCA}$ |
|---|---|---|---|---|---|
| 0.000 | 90.2110 | 0.241 | 0.242 | 0.131 | 0.816 |
| 0.010 | 92.5415 | 0.235 | 0.274 | 0.132 | 0.862 |
| 0.020 | 94.9956 | 0.228 | 0.332 | 0.134 | 0.971 |
| 0.025 | 96.2721 | 0.225 | 0.386 | 0.135 | 1.079 |
| 0.030 | 97.5834 | 0.222 | 0.500 | 0.137 | 1.270 |
| 0.035 | 98.9310 | 0.219 | 0.747 | 0.139 | 1.498 |
| 0.040 | 100.3162 | 0.215 | 1.028 | 0.141 | 1.583 |

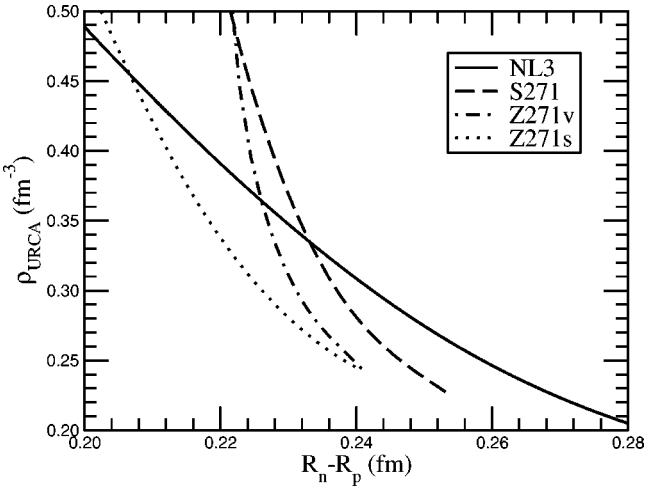


FIG. 2. Threshold density for the direct URCA process versus the predicted neutron skin $(R_n$-$R_p)$ of $^{208}$Pb. Parameter sets NL3, S271, and Z271v use a nonzero value for $\Lambda_v$ while Z271s uses a nonzero $\Lambda_s$.

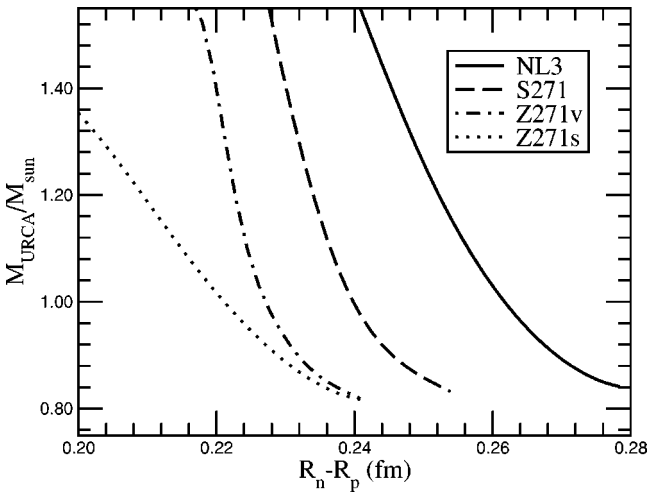


FIG. 3. Threshold neutron-star mass for the direct URCA process versus the predicted neutron skin ($R_n$-$R_p$) of $^{208}$Pb. Parameter sets NL3, S271, and Z271v use a nonzero value for $\Lambda_v$ while Z271s uses a nonzero $\Lambda_s$.

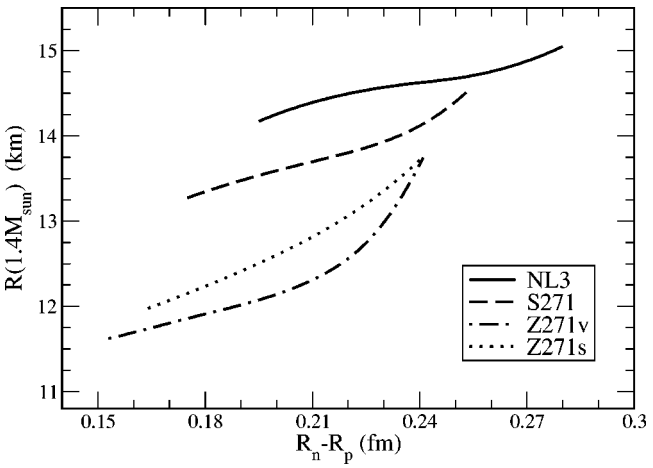


FIG. 4. Radius of a $1.4M_\odot$ neutron star versus the predicted neutron skin ($R_n$-$R_p$) of $^{208}$Pb. Parameter sets NL3, S271, and Z271v use a nonzero value for $\Lambda_v$ while Z271s uses a nonzero $\Lambda_s$.

occurs at low baryon densities. Indeed, parameter sets with neutron skins of $R_n - R_p \gtrsim 0.24$ fm yield a relative low URCA density of $\rho_{\rm URCA} \lesssim 0.30$ fm$^{-3}$. This density is only a factor of 2 larger than normal nuclear matter saturation density ($\rho_0 \approx 0.15$ fm$^{-3}$). In contrast, if $R_n - R_p \lesssim 0.21$ fm, the onset for the URCA process is above $3\rho_0$.

The structure of spherical neutron stars in hydrostatic equilibrium is solely determined by the equation of state of neutron-rich matter in beta equilibrium. Having specified the equation of state, we determine the mass of neutron stars that may cool via the direct URCA process by integrating the Tolman-Oppenheimer-Volkoff equations. Our treatment of the low-density crust, where the matter in the star is nonuniform, will be discussed in a later work [31]. This region, however, has almost no effect on neutron-star masses. As mentioned earlier, we consider matter composed of neutrons, protons, muons, and (massless) electrons. In Fig. 3 we display, as a function of the neutron skin in $^{208}$Pb, the mass of a neutron star whose central density equals the URCA density ($\rho_{\rm URCA}$) of Fig. 2. Neutron stars with larger masses, and thus higher central densities, will cool by the direct URCA process; those with lower masses will not. There is an obvious trend for this threshold mass to decrease with increasing $R_n - R_p$. Recall that the onset for URCA cooling in models with large neutron skins occurs at low baryon densities, thus lower ''URCA masses.'' If the neutron skin of $^{208}$Pb is less than about $R_n - R_p \lesssim 0.20$ fm, then all parameter sets considered in this work predict that a neutron star of $1.4M_\odot$ will not undergo URCA cooling. Conversely, if $R_n - R_p \gtrsim 0.25$ fm, then all parameter sets allow URCA cooling for $1.4M_\odot$ neutron star. Note that all well-measured neutron stars have masses near $1.4M_\odot$ [32]. The threshold neutron star mass for the direct URCA process, $M_{\rm URCA}$, depends on both the ''critical'' URCA density $\rho_{\rm URCA}$ (of Fig. 2) and on the equation of state at low and high densities. Yet the neutron skin of $^{208}$Pb constrains only the low-density EOS [24], thereby generating the model dependence displayed by Fig. 3. In particular, the radius of a neutron star, although correlated to $R_n - R_p$, is not determined uniquely by it [28]. This suggests that models with a stiff EOS at high density, such as the NL3 parameter set, will yield neutron stars with relatively large radii and low central densities. This implies, for example, that for a fixed central density of $\rho_{\rm URCA} = 0.3$ fm$^{-3}$, the NL3 set (with large radii) generates an URCA mass of $M_{\rm URCA} \simeq 1.4M_\odot$; in contrast, the softer Z271s set (with small radii) yields an URCA mass of only $M_{\rm URCA} \simeq 1M_\odot$. Equivalently, to make a $M_{\rm URCA} = 1.4M_\odot$ neutron star the NL3 set requires an interior density of $\rho_{\rm URCA} = 0.3$ fm$^{-3}$, while a central density almost twice as large is needed for the Z271s set to generate the same mass neutron star. These facts suggest that an accurate measurement of neutron-star radii may reduce the model dependence (i.e., the spread) observed in Fig. 3. Yet even without further constraints the spread is relatively small and a measurement of $R_n - R_p$ in $^{208}$Pb may still prove decisive.

We conclude this section with a brief comment on two recent references to the isolated neutron star RX J185635-3754 that suggest, as a result of a revised distance measurement, a rather stiff EOS [33,34]. In Ref. [34] Braje and Romani constrain the radius of a $1.5M_\odot$ neutron star to the relatively narrow range of $R = 13.7 \pm 0.6$ km [34]. If confirmed, such a ''large'' neutron-star radius will exclude most soft equations of state [25]. In Ref. [33] Walter and Lattimer suggest the more conservative limit for RX J185635-3754 of $M \simeq (1.7 \pm 0.4)M_\odot$ and $R \simeq 11.4 \pm 2.0$ km. These values exclude only the softest equations of state [25].

To make contact with the above two references, we display in Fig. 4 the radius of a $1.4M_\odot$ neutron star as a function of the neutron skin of $^{208}$Pb. While the figure shows a definite correlation—$R(1.4M_\odot)$ grows with increasing $R_n$-$R_p$—a model dependence develops because the radius of a $1.4M_\odot$ neutron star depends on the EOS at low and high densities while $R_n$ is insensitive to the high-density component of the EOS. Yet this model dependence could be reduced from an accurate mass-radius determination. Although a stiff EOS does not guarantee a large neutron radius in

$^{208}$Pb, a large neutron star radius is suggestive of a large $R_n$ which, as we have argued earlier, should allow the direct URCA cooling of a $1.4M_\odot$ neutron star. This suggestion appears to be in agreement with the young age of RX J185635-3754 which, at $5\times10^5$ years [33], appears to require some form of enhanced cooling [34]. Thus, the upcoming measurement of the neutron radius in $^{208}$Pb, when combined with a mass-radius determination, should place stringent constraints on the EOS.

## IV. SUMMARY AND CONCLUSIONS

Recent x-ray observations suggest that some neutron stars cool quickly. This enhanced cooling could arise from the direct URCA process—which requires a high proton fraction—or from the beta decay of additional hadrons in dense matter, such as pions, kaons, hyperons, or quarks. Yet it seems unlikely that x-ray observations alone will determine the origin of the enhanced cooling.

In this work we propose to use a laboratory experiment to constrain the direct URCA process in neutron stars. The Parity Radius Experiment at the Jefferson Laboratory [22,23] aims to measure the neutron radius of $^{208}$Pb accurately and model independently via parity-violating electron scattering. For the direct URCA process to be realized, the equilibrium proton fraction in the star must be large. The equilibrium proton fraction is determined by the symmetry energy, whose density dependence can be strongly constrained through a measurement of the neutron radius in $^{208}$Pb. Such a measurement could provide a reliable extrapolation of the proton fraction to higher densities. Thus, predictions for the neutron radius in $^{208}$Pb have been correlated to the proton fraction in dense neutron-rich matter by using a wide range of relativistic effective-field theory models. We find that models with a neutron skin in $^{208}$Pb of $R_n-R_p\lesssim0.20$ fm generate proton fractions that are too small to allow the direct URCA process in $1.4M_\odot$ neutron stars. Conversely, if $R_n-R_p\gtrsim0.25$ fm, then all models predict the URCA cooling of $1.4M_\odot$ stars.

While this paper has focused on relativistic effective field-theory models, we expect our conclusions to be general and applicable to other approaches, both relativistic and nonrelativistic. For example, the nonrelativistic equation of state of Friedman and Pandharipande [16] predicts too small a proton fraction for URCA cooling to be possible. Moreover, this equation of state yields a neutron skin in $^{208}$Pb of only $R_n-R_p=0.16\pm0.02$ fm [24]. Thus, these results are fully consistent with Fig. 3 that predicts no URCA cooling for such a small value of $R_n-R_p$.

The equation of state considered in this work consists of matter composed of neutrons, protons, electrons, and muons in beta equilibrium; no exotic component was invoked. Further, no explicit proton or neutron pairing was considered. Nucleon superfluidity is an accepted phenomenon in nuclear physics and superfluid gaps are important for the cooling of neutron stars [14]. Thus, the study of pairing gaps in relativistic effective-field theories is an important area of future work; first steps in this direction have been taken in Ref. [35]. In particular, the proton-pairing gap in matter with a high proton concentration must be computed [15].

In summary, the feasibility of enhanced cooling of neutron stars via the direct URCA process was studied by correlating the proton fraction in dense, neutron-rich matter to the neutron skin of $^{208}$Pb. Thus, a measurement of the neutron radius in $^{208}$Pb may become vital for confirming (or dismissing) the direct URCA cooling of neutron stars. If direct URCA cooling is ruled out, then observations of enhanced cooling may provide strong evidence in support of exotic states of matter, such as meson condensates and quark matter, at the core of neutron stars.

## ACKNOWLEDGMENTS

This work was supported by the U.S. DOE under Contract Nos. DE-FG02-87ER40365 and DE-FG05-92ER40750.

[1] B. Jegerlehner, F. Neubig, and G. Raffelt, Phys. Rev. D **54**, 1194 (1996).
[2] C.J. Pethick, Rev. Mod. Phys. **64**, 1133 (1992).
[3] P. Slane, D.J. Helfund, and S.S. Murray, astro-ph/0204151, Astrophys. J. (to be published).
[4] G.G. Pavlov, O.Y. Kargaltsev, D. Sanwal, and G.P. Garmire, Astrophys. J. Lett. **554**, L189 (2001).
[5] J.P. Halpern and F.Y.H. Wang, Astrophys. J. **477**, 905 (1997).
[6] R. Wijnands, M. Guainazzi, M. van der Kils, and M. Mendez, Astrophys. J. Lett. **573**, L45 (2002).
[7] M. Colpi, U. Geppert, D. Page, and A. Possenti, Astrophys. J. Lett. **548**, L175 (2001).
[8] V.E. Zavlin, J. Trümper, and G.G. Pavlov, Astrophys. J. **525**, 959 (1999).
[9] J.A. Pons, J.A. Miralles, M. Prakash, and J.M. Lattimer, Astrophys. J. **553**, 382 (2001).
[10] Madappa Prakash, Manju Prakash, James M. Lattimer, and C.J. Pethick, Astrophys. J. Lett. **390**, L77 (1992).
[11] P. Jaikumar and M. Prakash, Phys. Lett. B **516**, 345 (2001); M. Prakash, Nucl. Phys. **A698**, 440 (2002).
[12] J.M. Lattimer, C.J. Pethick, M. Prakash, and P. Haensel, Phys. Rev. Lett. **66**, 2701 (1991).
[13] L.B. Leinson, Nucl. Phys. **A707**, 543 (2002).
[14] D.G. Yakovlev, A.D. Kaminker, P. Haensel, and O.Y. Gnedin, astro-ph/0204233.
[15] S. Tsuruta, M.A. Teter, T. Takatsuka, T. Tatsumi, and R. Tamagaki, Astrophys. J. Lett. **571**, L143 (2002); astro-ph/0204508.
[16] B. Friedman and V.R. Pandharipande, Nucl. Phys. **A361**, 502 (1981).
[17] D.G. Yakovlev, A.D. Kaminker, and K.P. Levenfish, Astron. Astrophys. **343**, 650 (1999).
[18] D. Page, M. Prakash, J.M. Lattimer, and Andrew W. Steiner, Phys. Rev. Lett. **85**, 2048 (2000).
[19] E. Flowers, M. Ruderman, and P. Sutherland, Astrophys. J. **205**, 541 (1976); A.D. Kaminker, P. Haensel, and D.G. Yakovlev, Astron. Astrophys. **373**, L17 (2001); S. Tsuruta, Phys. Rep. **292**, 1 (1998).

[20] T. Takatsuka and R. Tamagaki, Prog. Theor. Phys. **97**, 345 (1997).
[21] Bao-An Li, Phys. Rev. Lett. **88**, 192701 (2002).
[22] Jefferson Laboratory Experiment E-00-003, R. Michaels, P. A. Souder, and G. M. Urciuoli, spokespersons.
[23] C.J. Horowitz, S.J. Pollock, P.A. Souder, and R. Michaels, Phys. Rev. C **63**, 025501 (2001).
[24] B. Alex Brown, Phys. Rev. Lett. **85**, 5296 (2000).
[25] J.M. Lattimer and M. Prakash, Astrophys. J. **550**, 426 (2001).
[26] B. Gwen, J. Piekarewicz, and C.J. Horowitz (unpublished).
[27] C.J. Horowitz and J. Piekarewicz, Phys. Rev. Lett. **86**, 5647 (2001).
[28] C.J. Horowitz and J. Piekarewicz, Phys. Rev. C **64**, 062802 (2001).
[29] H. Müller and B.D. Serot, Nucl. Phys. **A606**, 508 (1996).
[30] G.A. Lalazissis, J. König, and P. Ring, Phys. Rev. C **55**, 540 (1997).
[31] C.J. Horowitz and J. Piekarewicz (unpublished).
[32] S.E. Thorsett and Deepto Chakrabarty, Astrophys. J. **512**, 288 (1999).
[33] F.M. Walter and J.M. Lattimer, astro-ph/0204199.
[34] T.M. Braje and R.W. Romani, astro-ph/0208069.
[35] D.T. Son, hep-ph/0204199; H. Kucharek and P. Ring, Z. Phys. A **339**, 23 (1991).